





## 11 **Abstract**

12 We illustrate the nonlinear relationships among anthropogenic  $\text{NO}_x$  emissions,  $\text{NO}_2$   
13 tropospheric vertical column densities (TVCDs), and  $\text{NO}_2$  surface concentrations using model  
14 simulations for July 2011 over the contiguous United States (CONUS). The variations of  $\text{NO}_2$   
15 surface concentrations and TVCDs are generally consistent and reflect well anthropogenic  $\text{NO}_x$   
16 emission variations for high-anthropogenic- $\text{NO}_x$  emission regions. For low-anthropogenic- $\text{NO}_x$   
17 emission regions, however, nonlinearity in the emission-TVCD relationship makes it difficult to  
18 use satellite observations to infer anthropogenic  $\text{NO}_x$  emission changes. The analysis is extended  
19 to 2003 – 2017. Similar variations of  $\text{NO}_2$  surface measurements and coincident satellite  $\text{NO}_2$   
20 TVCDs over urban regions are in sharp contrast to the large variation differences between surface  
21 and satellite observations over rural regions. We find a continuous decrease of anthropogenic  
22  $\text{NO}_x$  emissions after 2011 by examining surface and satellite measurements in CONUS urban  
23 regions, but the decreasing rate is lower by 9% - 46% than the pre-2011 period.

24



## 25 1. Introduction

26 Anthropogenic emissions of nitrogen oxides ( $\text{NO}_x = \text{NO}_2 + \text{NO}$ ) adversely affect the  
27 environment, not only because of their direct detrimental impacts on human health (Greenberg et  
28 al., 2016; Greenberg et al., 2017; Heinrich et al., 2013; Weinmayr et al., 2009), but also their  
29 fundamental roles in the formation of ozone, acid rain, and fine particles which are unfavorable to  
30 human health, ecosystem stabilities, and climate change (Crouse et al., 2015; Kampa and  
31 Castanas, 2008; Myhre et al., 2013; Pandey et al., 2005; Singh and Agrawal, 2007). About 48.8  
32 Tg N  $\text{yr}^{-1}$  of  $\text{NO}_x$  are emitted globally from both anthropogenic (77%) and natural (23%) sources,  
33 such as fossil fuel combustion, biomass and biofuel burning, soil bacteria, and lightning (Seinfeld  
34 and Pandis, 2016). 3.85 Tg N and 0.24 Tg N of anthropogenic and natural  $\text{NO}_x$ , respectively,  
35 were emitted from the U.S. in 2014 on the basis of the 2014 National Emission Inventory  
36 (NEI2014); vehicle sources and fuel combustions accounted for 93% of the total anthropogenic  
37  $\text{NO}_x$  emissions (EPA, 2017).

38 The U.S. anthropogenic  $\text{NO}_x$  emissions during the 2010s declined dramatically compared to  
39 the mid-2000s (EPA, 2018; Xing et al., 2013) due to stricter air quality regulations and emission  
40 control technology improvements, such as the phase-in of Tier II vehicles during 2004 – 2009 and  
41 the switch of power plants from coal to natural gas (De Gouw et al., 2014; McDonald et al.,  
42 2018). The overall reduction (about 30% - 50%) of anthropogenic  $\text{NO}_x$  emissions from the mid-  
43 2000s to the 2010s was corroborated by observed decreasing of vehicle  $\text{NO}_x$  emission factors,  
44  $\text{NO}_2$  surface concentrations, nitrate wet deposition flux, and  $\text{NO}_2$  tropospheric vertical column  
45 densities (TVCDs) (Bishop and Stedman, 2015; Li et al., 2018; McDonald et al., 2018; Miyazaki  
46 et al., 2017; Russell et al., 2012; Tong et al., 2015). However, the detailed  $\text{NO}_x$  emission changes  
47 after the Great Recession (from December 2007 to June 2009) are highly uncertain. On the one  
48 hand, the U.S. Environmental Protection Agency (EPA) estimated that the Great Recession had a



49 slight impact on the anthropogenic NO<sub>x</sub> emission trend, and the anthropogenic NO<sub>x</sub> emissions  
50 decreased steadily from 2002 to 2017 (Figure S1), although the emission decrease rate slowed  
51 down by about 20% after 2010 (-5.8% yr<sup>-1</sup> for 2002 – 2010, and -4.7% yr<sup>-1</sup> for 2010 – 2017,  
52 Table 1) (EPA, 2018). Fuel-based emission estimates in Los Angeles also showed a steady  
53 decrease of anthropogenic NO<sub>x</sub> emissions after 2000 and a small impact of the Great Recession  
54 on anthropogenic NO<sub>x</sub> emission decrease trend (Hassler et al., 2016). The continuous decrease of  
55 anthropogenic NO<sub>x</sub> emissions was consistent with the ongoing reduction of vehicle emissions  
56 (McDonald et al., 2018). On the other hand, Miyazaki et al. (2017) and Jiang et al. (2018) found  
57 that the U.S. NO<sub>x</sub> emissions derived from satellite NO<sub>2</sub> TVCDs, including OMI (the Ozone  
58 Monitoring Instrument), SCIAMACHY (SCanning Imaging Absorption SpectroMeter for  
59 Atmospheric CHartography), and GOME-2A (Global Ozone Monitoring Experiment – 2 onboard  
60 METOP-A), were almost flat from 2010 - 2015 and suggested that the decrease of NO<sub>x</sub> emissions  
61 was only significant before 2010, which was completely different from the bottom-up and fuel-  
62 based emission estimates.

63 A complicating factor in inferring anthropogenic NO<sub>x</sub> emission trends from the observations  
64 of NO<sub>2</sub> surface concentrations and satellite NO<sub>2</sub> TVCDs is the nonlinearity in NO<sub>x</sub> chemistry (Gu  
65 et al., 2013; Gu et al., 2016). Although the decrease rates of both NO<sub>2</sub> surface concentrations and  
66 coincident OMI NO<sub>2</sub> TVCDs slowed down after the Great Recession over the United States,  
67 Tong et al. (2015), Lamsal et al. (2015) and Jiang et al. (2018) found that the slowdown of the  
68 decrease rates derived from NO<sub>2</sub> surface concentrations is 12% - 79% less than those of NO<sub>2</sub>  
69 TVCDs (Table 1). Secondly, the slowdown of the decrease rates of NO<sub>2</sub> surface concentrations  
70 and OMI TVCDs over cities and power plants (Russell et al., 2012; Tong et al., 2015) is  
71 significantly less than those over the whole contiguous United States (CONUS) (Jiang et al.,  
72 2018; Lamsal et al., 2015). Moreover, Zhang et al. (2018) found that filtering out lightning-



73 affected measurements could significantly improve the comparison of NO<sub>2</sub> surface concentration  
74 and OMI NO<sub>2</sub> TVCD trends over the CONUS.

75 In this study, we carefully investigate the relationships among anthropogenic NO<sub>x</sub> emissions,  
76 NO<sub>2</sub> surface concentrations, and NO<sub>2</sub> TVCDs over the CONUS and evaluate the impact of the  
77 relationships on inferring anthropogenic NO<sub>x</sub> emission changes and trends from surface and  
78 satellite observations. Section 2 describes the model and datasets used in this study, including the  
79 Regional chemistry and transport Model (REAM), the EPA Air Quality System (AQS) NO<sub>2</sub>  
80 surface observations, and NO<sub>2</sub> TVCD products from OMI, GOME-2A, GOME-2B (GOME2  
81 onboard METOP-B), and SCIAMACHY. In Section 3, we examine the nonlinear relationships  
82 among anthropogenic NO<sub>x</sub> emissions, NO<sub>2</sub> surface concentrations, and NO<sub>2</sub> TVCDs using model  
83 simulations. Accounting for the effects of chemical nonlinearity, we then investigate the  
84 anthropogenic NO<sub>x</sub> emission trends and changes from 2003 – 2017 over the CONUS. Finally,  
85 section 4 gives a summary of the study.

## 86 **2. Model and Data Description**

### 87 **2.1 REAM**

88 The REAM model has been applied and evaluated in many research applications including  
89 ozone simulation and forecast, emission inversion and evaluations, and mechanical studies of  
90 chemical and physical processes (Alkuwari et al., 2013; Cheng et al., 2017; Cheng et al., 2018;  
91 Choi et al., 2008a; Choi et al., 2008b; Gu et al., 2013; Gu et al., 2014; Koo et al., 2012; Liu et al.,  
92 2012; Liu et al., 2014; Wang et al., 2007; Yang et al., 2011; Zhang et al., 2017; Zhang et al.,  
93 2018; Zhang and Wang, 2016; Zhao and Wang, 2009; Zhao et al., 2009a; Zhao et al., 2010).  
94 REAM used in this work has 30 vertical layers in the troposphere, and the horizontal resolution is  
95 36 × 36 km<sup>2</sup>. The model is driven by meteorology fields from a Weather and Research



96 Forecasting (WRF, version 3.6) model simulation initialized and constrained by the NCEP  
97 coupled forecast system model version 2 (CFSv2) products (Saha et al., 2011). The chemistry  
98 mechanism is based on GEOS-Chem v11.01 with updated reaction rates and aerosol uptake of  
99 isoprene nitrates (Fisher et al., 2016). Chemistry boundary conditions and initializations are from  
100 a GEOS-Chem ( $2^\circ \times 2.5^\circ$ ) simulation. Hourly anthropogenic emissions on weekdays are based on  
101 the 2011 National Emission Inventory (NEI2011), while weekend anthropogenic emissions are  
102 set to be two-thirds of the weekday emissions (Beirle et al., 2003; Choi et al., 2012). Biogenic  
103 VOC emissions are estimated using the Model of Emissions of Gases and Aerosols from Nature  
104 (MEGAN) v2.10 (Guenther et al., 2012).  $\text{NO}_x$  emissions from soils are based on the Yienger and  
105 Levy (YL) scheme (Li et al., 2019; Yienger and Levy, 1995).

## 106 **2.2 Satellite $\text{NO}_2$ TVCDs**

107 In this study, we use  $\text{NO}_2$  TVCD products from four satellite measurements in the past  
108 decade, including SCIAMACHY, GOME-2A, GOME-2B, and OMI, the spectrometers onboard  
109 sun-synchronous satellites to monitor atmospheric trace gases. The SCIAMACHY onboard the  
110 Environmental Satellite (ENVISAT) has an equator overpass time of 10:00 Local time (LT) and a  
111 nadir pixel resolution of  $60 \times 30 \text{ km}^2$ . The GOME-2 instruments on Metop-A (named as GOME-  
112 2A) and Metop-B (GOME-2B) satellites cross the equator at 9:30 LT and have a nadir resolution  
113 of  $80 \times 40 \text{ km}^2$ . After July 15, 2013, the nadir resolution of GOME-2A became  $40 \times 40 \text{ km}^2$  with  
114 a smaller scanning swath. The OMI onboard the EOS-Aura satellite has a nadir resolution of  $24 \times$   
115  $13 \text{ km}^2$  and overpasses the equator around 13:45 LT. More detailed information about these  
116 instruments is summarized in Table S1. These instruments measure transmitted, backscattered,  
117 and reflected radiation from the atmosphere in the ultraviolet and visible wavelength. The  
118 radiation measurements in the wavelength of 402 - 465 nm are then used to retrieve  $\text{NO}_2$  VCDs.  
119 The retrieval process consists of three steps: 1) converting radiation observations to  $\text{NO}_2$  slant  
120 column densities (SCDs) by using the Differential Optical Absorption Spectroscopy (DOAS)



121 spectral fitting method; 2) separating tropospheric SCDs and stratospheric SCDs from the total  
122 NO<sub>2</sub> SCDs; 3) dividing the NO<sub>2</sub> tropospheric SCDs by the tropospheric air mass factors (AMF) to  
123 compute VCDs.

124 The product archives we use in this study include GOME-2B (TM4NO2A v2.3),  
125 SCIAMACHY (QA4ECV v1.1), GOME-2A (QA4ECV v1.1), OMI (QA4ECV v1.1, hereafter  
126 referred to as OMI-QA4ECV), OMNO2 (SPv3, hereafter referred to as OMI-NASA), and the  
127 Berkeley High-Resolution NO<sub>2</sub> products (v3.0B, hereafter referred to as OMI-BEHR). OMI-  
128 BEHR uses the tropospheric SCDs from OMI-NASA products but updates some inputs for the  
129 tropospheric AMF calculation (Laughner et al., 2018). These product archives have been  
130 previously validated (Boersma et al., 2018; Drosoglou et al., 2017; Drosoglou et al., 2018;  
131 Krotkov et al., 2017; Laughner et al., 2018; Wang et al., 2017; Zara et al., 2018). Generally, the  
132 pixel-size uncertainties of these products are > 30% over polluted regions under clear-sky  
133 conditions. We summarize the basic information about these products in Table S2. To keep the  
134 high quality and sampling consistency of NO<sub>2</sub> TVCD datasets, we chose pixel-size NO<sub>2</sub> TVCD  
135 data using the criteria listed in Table S3. After the selection, we re-grid the pixel-size data into the  
136 REAM 36 × 36 km<sup>2</sup> grid cells and calculate the seasonal means of each grid cell with  
137 corresponding daily values on weekdays (winter: January, February, and December; spring:  
138 March, April, and May; summer: June, July, and Autumn; autumn: September, October, and  
139 November). We excluded weekend data in this study to minimize the impacts of weekend NO<sub>x</sub>  
140 emission reduction, leading to different NO<sub>2</sub> TVCDs between weekdays and weekends (Figure  
141 S2).

142 Satellite TVCD measurements can show large variations and apparent discontinuities due in  
143 part to the effects of cloud, lightning NO<sub>x</sub>, the shift of satellite pixel coverage, and retrieval  
144 uncertainties (Figure S2; e.g., (Boersma et al., 2018; Zhang et al., 2018)). However, continuous  
145 and consistent measurements are required for reliable trend analyses. In addition to the criteria of



146 data selection in Table S3, we compute the seasonal relative 90<sup>th</sup> percentile confidence interval,  
147 defined as  $RCI = (X(95^{th} \text{ percentile}) - X(5^{th} \text{ percentile})) / \text{mean}(X)$ , where X is the daily NO<sub>2</sub>  
148 TVCD for a given season. To compute the seasonal trend, we require that RCI is < 50% for the  
149 selected season every year in the analysis period (Table S3). About 45% of data are removed as a  
150 result.

### 151 **2.3 Surface NO<sub>2</sub> measurements**

152 Hourly surface NO<sub>2</sub> measurements from 2003 - 2017 are from the EPA AQS monitoring  
153 network (archived on <https://www.epa.gov/outdoor-air-quality-data>). Most AQS monitoring sites  
154 use the Federal Reference Method (FRM) — gas-phase chemiluminescence to measure NO<sub>2</sub>. Few  
155 sites use the Federal Equivalent Method (FEM) – photolytic-chemiluminescence or the Cavity  
156 Attenuated Phase Shift Spectroscopy (CAPS) method. FRM and FEM are indirect methods, in  
157 which NO<sub>2</sub> is first converted to NO and then NO is measured through chemiluminescence  
158 measurement of NO<sub>2</sub>\* produced by NO + O<sub>3</sub>. The difference is that FRM uses heated  
159 reducers/catalysts for the conversion of NO<sub>2</sub> to NO and FEM uses photolysis of NO<sub>2</sub> to NO. The  
160 conversion to NO in the FRM instruments is not specific to NO<sub>2</sub>, and non-NO<sub>x</sub> active nitrogen  
161 compounds (NO<sub>z</sub>) can also be reduced by the catalysts, which would cause high biases of NO<sub>2</sub>  
162 measurements, while the FEM method is sensitive to the photolysis conversion efficiency of NO<sub>2</sub>  
163 to NO (Beaver et al., 2012; Beaver et al., 2013; Lamsal et al., 2015). The CAPS method directly  
164 determines NO<sub>2</sub> concentrations based on a NO<sub>2</sub>-induced phase shift measured by a photodetector.  
165 The CAPS instrument operates at a wavelength of about 450 nm and may overestimate NO<sub>2</sub>  
166 concentrations due to absorption of other molecules at the same wavelength (Beaver et al., 2012;  
167 Beaver et al., 2013; Kebabian et al., 2005).

168 Due to the different characteristics of the above three methods and demonstrated biases  
169 between the FRM and the FEM by Lamsal et al. (2015), we firstly investigate the measurement



170 discrepancies among the above three methods. There are three sites having FRM and FEM  
171 measurements simultaneously during some periods from 2013 - 2014, two sites having both FRM  
172 and CAPS data during some periods from 2015 – 2016, and one site using all three measurement  
173 methods during some periods in 2015. Figure S3 shows the hourly averaged ratios of FEM and  
174 CAPS to FRM data, respectively, for 4 seasons during 2013 – 2016. The CAPS/FRM ratios are in  
175 the range of 0.94 – 1.06 and the FEM/FRM ratios of 0.86 – 1.11. Furthermore, Zhang et al.  
176 (2018) discussed that the relative trends are not affected by scaling the observation data. As in the  
177 work by Zhang et al. (2018), we analyze the relative trends in the surface NO<sub>2</sub> data. We,  
178 therefore, did not scale the FRM data. At sites with FEM or CAPS measurements, we use these  
179 measurements in place of FRM data. If both FEM and CAPS data are available, we use the  
180 averages of the two datasets.

181 Since NO<sub>2</sub> surface concentrations have significant diurnal variations (Figure S4), we choose  
182 the data at 9:00-10:00 LT for comparison with GOME-2A/2B data, 10:00-11:00 LT for  
183 comparison with SCIAMACHY data, and 13:00-14:00 LT for OMI data. The seasonal  $RCI <$   
184 50% requirement is also used here to be consistent with the analysis of satellite TVCD data. We  
185 also require that the measurement site must have valid measurements in the aforementioned 3  
186 hours for at least one season from 2003 – 2017. The locations of the 179 selected sites using the  
187 site selection criteria are shown in Figure 1. The region definitions follow the U.S. Census Bureau  
188 ([https://www2.census.gov/geo/pdfs/maps-data/maps/reference/us\\_regdiv.pdf](https://www2.census.gov/geo/pdfs/maps-data/maps/reference/us_regdiv.pdf)).



## 189 **3. Results and Discussions**

### 190 **3.1 Nonlinear relationships among anthropogenic NO<sub>x</sub> emissions, NO<sub>2</sub> surface** 191 **concentrations, and NO<sub>2</sub> TVCDs**

192 NO<sub>2</sub> surface concentrations and NO<sub>2</sub> TVCD are not linearly correlated with NO<sub>x</sub> emissions  
193 due in part to chemical nonlinearity (Gu et al., 2013; Lamsal et al., 2011). Therefore, it is  
194 necessary to first investigate the nonlinearities among NO<sub>x</sub> emissions, NO<sub>2</sub> surface  
195 concentrations, and TVCDs over the CONUS before we compare the trends between NO<sub>2</sub> surface  
196 concentrations and TVCDs. The nonlinearity between NO<sub>x</sub> emission and NO<sub>2</sub> TVCD is analyzed  
197 by examining the local sensitivity of NO<sub>2</sub> TVCD to NO<sub>x</sub> emissions (Gu et al., 2013; Lamsal et al.,  
198 2011; Tong et al., 2015), which is defined as  $\beta$  in Equation (1). We further define  $\gamma$  as the  
199 sensitivity of NO<sub>2</sub> surface concentration to NO<sub>x</sub> emission:

$$200 \quad \frac{\Delta E}{E} = \beta \frac{\Delta \Omega}{\Omega} \quad (1)$$

$$201 \quad \frac{\Delta E}{E} = \gamma \frac{\Delta c}{c} \quad (2)$$

202 where  $E$  denotes NO<sub>x</sub> emission and  $\Delta E$  denotes the change of NO<sub>x</sub> emission;  $\Omega$  denotes NO<sub>2</sub>  
203 TVCD,  $c$  denotes surface NO<sub>2</sub> concentration, and  $\Delta \Omega$  and  $\Delta c$  denote the corresponding changes.

204 We computed  $\beta$  and  $\gamma$  values for July 2011 over the CONUS using REAM. To compute  
205 local  $\beta$  and  $\gamma$  values, we added another independent group of chemistry species (“group 2”) in  
206 REAM in order to compute the standard and sensitivity simulations concurrently. The original  
207 chemical species in the model (“group 1”) were used in the standard simulation. For group 2  
208 chemical species, anthropogenic NO<sub>x</sub> emissions were reduced by 15%. In model simulation, we  
209 first computed the advection of group 1 tracers. The horizontal tracer fluxes were therefore



210 available. All influxes into a grid cell for group 2 tracer simulation were from group 1 tracer  
211 simulation; only outfluxes were computed using group 2 tracers. The outflux was one way in that  
212 nitrogen species were transported out but the transport did not affect adjacent grid cells because  
213 the influxes were from group 1 tracer simulation. Using this procedure, the effects of  
214 anthropogenic  $\text{NO}_x$  emission reduction were localized. The  $\beta$  and  $\gamma$  values were computed by the  
215 ratio of TVCD and surface concentration changes to 15% change of anthropogenic  $\text{NO}_x$   
216 emissions, respectively.

217 Figure 2 shows the distributions of our  $\beta$  and  $\gamma$  ratios as a function of anthropogenic  $\text{NO}_x$   
218 emissions for July 2011 over the CONUS. Results essentially the same as Figure 2 were obtained  
219 when a perturbation of 10% was used for anthropogenic  $\text{NO}_x$  emissions. While the model  
220 simulation is for one summer month, several key points on the surface and column concentration  
221 sensitivities to anthropogenic  $\text{NO}_x$  emissions have implications for comparing the trends of AQS  
222 and satellite TVCD data. (1) Both  $\beta$  and  $\gamma$  values are negatively correlated with anthropogenic  
223  $\text{NO}_x$  emissions due to chemical nonlinearity and background  $\text{NO}_x$  contributions (Gu et al., 2016;  
224 Lamsal et al., 2011). It is consistent with the distribution of  $\beta$  as a function of  $\text{NO}_x$  emissions in  
225 China (Gu et al., 2013), although the  $\beta$  ratios for the US are generally larger than for China due  
226 primarily to different emission distributions of  $\text{NO}_x$  and VOCs and regional circulation patterns  
227 (Zhao et al., 2009b). (2) The uncertainties of  $\beta$  and  $\gamma$  values increase significantly as  
228 anthropogenic  $\text{NO}_x$  emissions decrease, which means regions with low anthropogenic  $\text{NO}_x$   
229 emissions are more sensitive to environmental conditions, such as  $\text{NO}_x$  transport from nearby  
230 regions which may even produce negative  $\beta$  and  $\gamma$  values. (3) The value of  $\gamma$  is generally less than  
231  $\beta$ , especially for low-anthropogenic- $\text{NO}_x$  emission regions, which reflects the significant  
232 contribution of free tropospheric  $\text{NO}_2$  to  $\text{NO}_2$  TVCD but not to  $\text{NO}_2$  surface concentrations. (4)  
233 The variations of  $\beta$  and  $\gamma$  values in anthropogenic  $\text{NO}_x$  emission bins tend to be larger at 10:00 –  
234 11:00 than at 13:00 – 14:00 LT, reflecting a stronger transport effect due to weaker chemical



235 losses at 10:00 – 11:00. (5) Both  $\beta$  and  $\gamma$  values are significantly less than 1 at 13:00 – 14:00 LT  
236 ( $\beta = 0.74$  and  $\gamma = 0.84$ ) when anthropogenic  $\text{NO}_x$  emissions are  $> 4 \times 10^{12}$  molecules  $\text{cm}^{-2} \text{s}^{-1}$ , but  
237 they are close to 1 at 10:00 – 11:00 LT ( $\beta = 0.96$  and  $\gamma = 1.02$ ), which reflect stronger chemistry  
238 nonlinearity at 13:00 – 14:00 than in the morning.

239 The largely varying  $\beta$  and  $\gamma$  values for anthropogenic  $\text{NO}_x$  emissions  $< 10^{11}$  molecules  $\text{cm}^{-2}$   
240  $\text{s}^{-1}$  imply that the trends derived from satellite TVCD data do not directly represent anthropogenic  
241  $\text{NO}_x$  emissions and that the variations of TVCD data may not be comparable to the corresponding  
242 surface  $\text{NO}_2$  concentrations. We define a region “urban” if anthropogenic  $\text{NO}_x$  emissions are  $>$   
243  $10^{11}$  molecules  $\text{cm}^{-2} \text{s}^{-1}$ . All the other regions are defined as “rural”. Figure 3 shows the  
244 distributions of anthropogenic  $\text{NO}_x$  emissions and urban and rural regions defined in this study.  
245 Such defined urban regions account for 69.8% of the total anthropogenic  $\text{NO}_x$  emissions over the  
246 CONUS, the trend of which is, therefore, representative of anthropogenic emission changes. A  
247 caveat is that some “urban” regions would become “rural” if anthropogenic  $\text{NO}_x$  emissions  
248 decreased after 2011 as the EPA anthropogenic  $\text{NO}_x$  emission trend suggested (Figure S1). In a  
249 sensitivity study, we define an urban region using a stricter criterion of anthropogenic  $\text{NO}_x$   
250 emissions  $> 2 \times 10^{11}$  molecules  $\text{cm}^{-2} \text{s}^{-1}$  and the analysis results are similar to those shown in the  
251 next section.

### 252 **3.2 Trend comparisons between $\text{NO}_2$ AQS surface concentrations and coincident** 253 **satellite $\text{NO}_2$ tropospheric VCD over urban and rural regions**

254 By using anthropogenic  $\text{NO}_x$  emissions of  $10^{11}$  molecules  $\text{cm}^{-2} \text{s}^{-1}$  as the threshold value, 157  
255 AQS sites are urban, and the rest 22 sites are rural. Their properties are summarized in Table 2.  
256 Figure 4 shows the relative annual variations of AQS  $\text{NO}_2$  surface measurements at 13:00 – 14:00  
257 and coincident OMI-QA4ECV  $\text{NO}_2$  TVCD data from 2005 – 2017 in each season for urban and  
258 rural regions. The contrast between the two regions is apparent in all seasons. For comparison



259 purposes, we scale the time series of TVCD and AQS surface NO<sub>2</sub> to their corresponding 2005  
260 values, and the resulting data are therefore unitless. Over urban regions, NO<sub>2</sub> surface  
261 concentrations are highly correlated with NO<sub>2</sub> TVCDs ( $\text{TVCD} = 1.03 \times \text{AQS} + 0.11$ ,  $R^2 = 0.98$ ),  
262 reflecting the comparable and stable  $\beta$  and  $\gamma$  values (Figure 2). However, over rural regions, the  
263 scaled TVCD data significantly deviate from AQS NO<sub>2</sub> data ( $\text{TVCD} = 1.15 \times \text{AQS} + 0.09$ ,  $R^2 =$   
264  $0.87$ ). It is noteworthy that the discrepancies between urban and rural data are smaller in winter  
265 than in spring, summer, and autumn due to a more dominant role of transport than chemistry and  
266 lower natural NO<sub>x</sub> emissions in winter.

267 We also examine the correlations of AQS NO<sub>2</sub> surface concentrations with coincident OMI-  
268 NASA, OMI-BEHR, SCIAMACHY, GOME-2A, and GOME-2B TVCD measurements. The  
269 results of OMI-NASA and OMI-BEHR are similar to those of OMI-QA4ECV (Figure 4).  
270 SCIAMACHY and GOME-2B TVCD observations at 9:00-11:00 LT also show large contrast  
271 between urban (SCIAMACHY:  $\text{TVCD} = 0.92 \times \text{AQS} - 0.005$ ,  $R^2 = 0.94$ ; GOME-2B:  $\text{TVCD} =$   
272  $0.54 \times \text{AQS} + 0.56$ ,  $R^2 = 0.96$ ) and rural regions (SCIAMACHY:  $\text{TVCD} = 0.77 \times \text{AQS} + 0.83$ ,  $R^2 =$   
273  $0.63$ ; GOME-2B:  $\text{TVCD} = 0.46 \times \text{AQS} + 0.73$ ,  $R^2 = 0.59$ ). The correlation of coincident  
274 GOME-2A NO<sub>2</sub> TVCD data with AQS surface concentrations is poor for rural ( $\text{TVCD} = 0.65 \times$   
275  $\text{AQS} + 0.56$ ,  $R^2 = 0.44$ ) and urban ( $\text{TVCD} = 0.31 \times \text{AQS} + 0.56$ ,  $R^2 = 0.21$ ) regions (Figure S5),  
276 which likely reflects the degradation of the GOME-2A instrument causing significant increase of  
277 NO<sub>2</sub> SCD uncertainties (Boersma et al., 2018). Therefore, we excluded GOME-2A in the analysis  
278 hereafter.

279 We further investigate the sensitivities of OMI-QA4ECV NO<sub>2</sub> TVCD relative annual  
280 variations from 2005 - 2017 to different anthropogenic NO<sub>x</sub> emissions over the CONUS in Figure  
281 5. We find clear flattening of NO<sub>2</sub> TVCD variations as anthropogenic NO<sub>x</sub> emissions decrease,  
282 which is consistent with the above analysis. Similar to Figure 4, the spread of TVCD variation is  
283 much less in winter than the other seasons. The differences between Figures 5 and 4 are due to a



284 much larger dataset used in the former than the latter. Only coincident AQS and OMI-QA4ECV  
285 data are used in Figure 4, but all OMI-KMNI data are used in Figure 5.

### 286 **3.3 Trend analysis of AQS NO<sub>2</sub> surface concentrations, satellite TVCDs, and** 287 **updated EPA NO<sub>x</sub> emissions**

288 We first updated the CEMS measurement data used in the EPA NO<sub>x</sub> emission trend datasets  
289 with the newest datasets obtained from <https://ampd.epa.gov/ampd/>. As shown in Figure S1, the  
290 updated CEMS data lead to a reduction of anthropogenic NO<sub>x</sub> emissions during the Great  
291 Recession (2008 – 2009) and a recovery period in 2010 – 2011. The sharp drop during the Great  
292 Recession and the flattening trend right after the Great Recession are captured by OMI NO<sub>2</sub> and  
293 SCIAMACHY TVCD products (Figures 4, 6, and S6) and AQS NO<sub>2</sub> surface measurements  
294 (Figures 4, 6, and S4) and are also noted by Russell et al. (2012) and Tong et al. (2015) (Table 1).

295 In Figure 6, we show the comparisons among the relative variations of the updated EPA  
296 anthropogenic NO<sub>x</sub> emissions, AQS NO<sub>2</sub> surface measurements at 10:00-11:00 and 13:00-14:00,  
297 and coincident satellite NO<sub>2</sub> TVCDs for urban regions in 4 seasons from 2003 to 2017. Also  
298 shown are the comparisons among the updated EPA anthropogenic NO<sub>x</sub> emissions and satellite  
299 NO<sub>2</sub> TVCDs. There are many more data points for the latter comparison because the data  
300 selection is no longer limited to those coincident with the AQS surface data, and therefore, the  
301 uncertainty spread is much lower. The comparisons, in general, show consistent results that the  
302 updated EPA anthropogenic NO<sub>x</sub> emissions, AQS surface measurements, and satellite TVCD  
303 data are in agreement. The agreement of decreasing trends among the datasets is just as good for  
304 the post-2011 period as the pre-2011 period. This result differs from Miyazaki et al. (2017) and  
305 Jiang et al. (2018), who suggested no significant decreasing trend for OMI TVCD data and  
306 inversed NO<sub>x</sub> emissions after 2010. The disagreement can be explained by the results of Figure 5.  
307 Including the low anthropogenic NO<sub>x</sub> emission regions leads to underestimates of NO<sub>x</sub> decreases.



308 Since the area of low anthropogenic NO<sub>x</sub> emission regions is larger than high anthropogenic NO<sub>x</sub>  
309 emission regions (Table 2), the arithmetic averaging will lead to a large weighting of rural  
310 observations, which do not reflect anthropogenic NO<sub>x</sub> emission changes. Miyazaki et al. (2017)  
311 and Jiang et al. (2018) included all regions in their analyses, but we exclude rural regions. Figure  
312 S6 shows the seasonal variations if the TVCDs over rural regions are included; the result shows a  
313 much lower decreasing rate of TVCDs over the CONUS. The much slower satellite TVCD trends  
314 for regions with low NO<sub>x</sub> emissions was previously discussed by Zhang et al. (2018). In addition,  
315 Miyazaki et al. (2017) and Jiang et al. (2018) conducted NO<sub>x</sub> emission inversions by using the  
316 Model for Interdisciplinary Research on Climate (MIROC)-Chem with a coarse resolution of 2.8°  
317 × 2.8°, which was insufficient to separate urban and rural regions and might distort predicted NO<sub>2</sub>  
318 TVCDs and inversed NO<sub>x</sub> emissions due to nonlinear effects (Valin et al., 2011; Yu et al., 2016),  
319 which is another possible reason for their find of flattening NO<sub>x</sub> emission trends after 2010.

320 We summarize the decreasing rates of NO<sub>2</sub> after the Great Recession in Table 3. To  
321 minimize the effect of the sharp decrease and the subsequent recovery, we chose to analyze the  
322 post-2011 period. Table 3 summarizes the results for each season, while Table 1 gives the  
323 averaged annual decreasing trends. Generally, Tables 1 and 3 confirm the continuous decreases of  
324 AQS surface observations, satellite NO<sub>2</sub> TVCD, and updated EPA anthropogenic NO<sub>x</sub> emissions  
325 after 2011 as in Figure 6, but decreasing rates are lower than the pre-2011 period. Over the AQS  
326 urban sites, the slowdown magnitudes are 9% for AQS surface observations and 20% - 40% for  
327 satellite NO<sub>2</sub> TVCD measurements, which may reflect in part smaller  $\gamma$  than  $\beta$  values (Table 2).  
328 Our estimated slowdown magnitudes are significantly lower than Lamsal et al. (2015) and Jiang  
329 et al. (2018) but comparable to the results by Tong et al. (2015) (Table 1). The agreement with  
330 Tong et al. (2015) is because we select urban AQS sites based on anthropogenic NO<sub>x</sub> emissions  
331 and they chose eight large cities, while Lamsal et al. (2015) and Jiang et al. (2018) used all AQS  
332 sites.



333 Over the CONUS urban regions, updated EPA anthropogenic NO<sub>x</sub> emissions show a  
334 slowdown of 22% compared to 29% - 46% for three OMI NO<sub>2</sub> TVCD products. The difference is  
335 partially due to the  $\beta$  ratio of  $2.3 \pm 0.9$  at 13:00 – 14:00 over the CONUS urban regions (Table 2).  
336 Satellite NO<sub>2</sub> TVCD measurement uncertainties also contribute to the difference. From 2013 –  
337 2017, GOME-2B NO<sub>2</sub> TVCDs decrease more than OMI products, especially in spring, autumn  
338 and winter (Tables 1 and 3). Finally, trend analyses in different regions (Figure 7 and Table S4)  
339 indicate that generally, the Midwest has the least slowdown of the decreasing rate for urban OMI  
340 NO<sub>2</sub> TVCD (-14% on average) after 2011 compared to the Northeast (-30%), South (-34%), and  
341 West (-28%).

342 The results presented in this study are qualitatively in agreement with the work by Silvern et  
343 al. (2019). The two studies were independent. Therefore, the foci of the studies are different  
344 despite reaching similar conclusions. While we focused on understanding the detailed data  
345 analysis of Jiang et al. (2018) and limited the use of model simulation results so that our results  
346 can be compared to the previous study directly, Silvern et al. (2019) relied more on multi-year  
347 model simulations. As a result, Silvern et al. (2019) can clearly identify the contributions of the  
348 NO<sub>2</sub> columns by natural emissions and make use of additional observations such as nitrate  
349 deposition fluxes. They also identified model biases in simulating the trends of NO<sub>2</sub> TVCDs by  
350 natural emissions. Our study, on the other hand, explored the data analysis procedure through  
351 which the trend of anthropogenic emissions can be derived from satellite observations and its  
352 limitations.

## 353 **4. Conclusions**

354 Using model simulations for July 2017, we demonstrate the nonlinear relationship of NO<sub>2</sub>  
355 surface concentration and TVCD with anthropogenic NO<sub>x</sub> emissions. Over low anthropogenic  
356 NO<sub>x</sub> emission regions, the ratios of anthropogenic NO<sub>x</sub> emission changes to the changes of



357 surface concentrations ( $\gamma$ ) and TVCDs ( $\beta$ ) have very large variations and  $\beta > \gamma \gg 1$ .  
358 Therefore, for the same emission changes, surface concentration and TVCD changes are much  
359 smaller and variable than urban regions, making it difficult to use the observations to directly  
360 infer anthropogenic  $\text{NO}_x$  emission trends. We find that defining urban regions where  
361 anthropogenic  $\text{NO}_x$  emissions are  $> 10^{11}$  molecules  $\text{cm}^{-2} \text{s}^{-1}$  and using surface and TVCD  
362 observations over these regions can infer the trends that can be compared with the EPA emission  
363 trend estimates.

364 We evaluate the anthropogenic  $\text{NO}_x$  emission variations from 2003 – 2017 over the CONUS  
365 by using satellite  $\text{NO}_2$  TVCD products from GOME-2B, SCIAMACHY, OMI-QA4ECV, OMI-  
366 NASA, and OMI-BEHR, over the urban regions of CONUS. We find broad agreements among  
367 the decreases of AQS  $\text{NO}_2$  surface observations, satellite  $\text{NO}_2$  TVCD products, and the EPA  
368 anthropogenic  $\text{NO}_x$  emissions with the CEMS dataset updated. After 2011, they all show a  
369 slowdown of the decreasing rates. Over the AQS urban sites,  $\text{NO}_2$  surface concentrations have a  
370 slowdown of 9% and OMI products show a slowdown of 20% - 40%. Over the CONUS urban  
371 regions, OMI TVCD products indicate a slowdown of 29% - 46%, and the updated EPA  
372 anthropogenic  $\text{NO}_x$  emissions have a slowdown of 22%. The different slowdown magnitudes  
373 between OMI TVCD products and the other two datasets may be caused by the nonlinear  
374 response of TVCD to anthropogenic emissions and the uncertainties of satellite measurements  
375 (e.g., GOME-2B TVCD data show a larger decreasing trend than OMI products from 2013 –  
376 2017).

377 We did not find observation evidence supporting the notion that anthropogenic  $\text{NO}_x$   
378 emissions have not been decreasing after the Great Recession. In future studies, we recommend  
379 that the nonlinear relationships of  $\text{NO}_x$  emissions with  $\text{NO}_2$  TVCD and surface concentration be



380 carefully evaluated when applying satellite and surface measurements to infer the changes of  
381 anthropogenic NO<sub>x</sub> emissions.

### 382 **Data availability**

383 The EPA AQS hourly surface NO<sub>2</sub> measurements are downloaded from  
384 [https://aqs.epa.gov/aqsweb/airdata/download\\_files.html#Raw](https://aqs.epa.gov/aqsweb/airdata/download_files.html#Raw). QA4ECV 1.1 NO<sub>2</sub> VCD products  
385 (OMI-QA4ECV, GOME-2A, and SCIAMACHY) are from <http://temis.nl/qa4ecv/no2col/data/>.  
386 GOME-2B NO<sub>2</sub> VCD products are from  
387 <http://www.temis.nl/airpollution/no2col/no2colgome2b.php>. OMI-BEHR and OMI-NASA  
388 archives are from <http://behr.cchem.berkeley.edu/DownloadBEHRData.aspx>. REAM simulation  
389 results for this study are available upon request.

### 390 **Author contribution**

391 JL and YW designed the study. JL conducted model simulations and data analyses with  
392 discussions with YW. JL and YW wrote the manuscript.

### 393 **Competing interests**

394 The authors declare that they have no conflict of interest.

### 395 **Acknowledgments**

396 This work was supported by the NASA ACMAP Program. We thank Ruixiong Zhang for  
397 discussions with J. Li. Thank Benjamin Wells, Alison Eyth, Lee Tooty from EPA, the EPA  
398 MOVES team, Betty Carter from COORDINATING RESEARCH COUNCIL, INC., Brian  
399 McDonald from NOAA, and Zhe Jiang from University of Science and Technology of China for  
400 helping us an understanding of the NEI MOVES mobile source emissions.



401 **References**

- 402 Alkuwari, F. A., Guillas, S., and Wang, Y.: Statistical downscaling of an air quality model using  
403 Fitted Empirical Orthogonal Functions, *Atmospheric environment*, 81, 1-10,  
404 10.1016/j.atmosenv.2013.08.031, 2013.
- 405 Beaver, M., Long, R., and Kronmiller, K.: Characterization and Development of Measurement  
406 Methods for Ambient Nitrogen Dioxide (NO<sub>2</sub>), National Air Quality Conference - Ambient Air  
407 Monitoring 2012, Denver, CO, US, 2012.
- 408 Beaver, M., Kronmiller, K., Duvall, R., Kaushik, S., Morphy, T., King, P., and Long, R.: Direct  
409 and Indirect Methods for the Measurement of Ambient Nitrogen Dioxide, AWMA Measurement  
410 Technologies meeting, Sacramento, CA, US, 2013.
- 411 Beirle, S., Platt, U., Wenig, M., and Wagner, T.: Weekly cycle of NO<sub>2</sub> by GOME measurements:  
412 A signature of anthropogenic sources, *Atmospheric Chemistry and Physics*, 3, 2225-2232,  
413 10.5194/acp-3-2225-2003, 2003.
- 414 Bishop, G. A., and Stedman, D. H.: Reactive nitrogen species emission trends in three light-  
415 /medium-duty United States fleets, *Environmental science & technology*, 49, 11234-11240,  
416 10.1021/acs.est.5b02392, 2015.
- 417 Boersma, K. F., Eskes, H. J., Richter, A., De Smedt, I., Lorente, A., Beirle, S., van Geffen, J. H.,  
418 Zara, M., Peters, E., and Roozendaal, M. V.: Improving algorithms and uncertainty estimates for  
419 satellite NO<sub>2</sub> retrievals: results from the quality assurance for the essential climate variables  
420 (QA4ECV) project, *Atmospheric Measurement Techniques*, 11, 6651-6678, 10.5194/amt-11-  
421 6651-2018, 2018.
- 422 Cheng, Y., Wang, Y., Zhang, Y., Chen, G., Crawford, J. H., Kleb, M. M., Diskin, G. S., and  
423 Weinheimer, A. J.: Large biogenic contribution to boundary layer O<sub>3</sub> - CO regression slope in  
424 summer, *Geophysical Research Letters*, 44, 7061-7068, 10.1002/2017GL074405, 2017.
- 425 Cheng, Y., Wang, Y., Zhang, Y., Crawford, J. H., Diskin, G. S., Weinheimer, A. J., and Fried, A.:  
426 Estimator of surface ozone using formaldehyde and carbon monoxide concentrations over the  
427 eastern United States in summer, *Journal of Geophysical Research: Atmospheres*, 123, 7642-  
428 7655, 10.1029/2018JD028452, 2018.
- 429 Choi, Y., Wang, Y., Yang, Q., Cunnold, D., Zeng, T., Shim, C., Luo, M., Eldering, A., Bucsela,  
430 E., and Gleason, J.: Spring to summer northward migration of high O<sub>3</sub> over the western North  
431 Atlantic, *Geophysical Research Letters*, 35, 10.1029/2007GL032276, 2008a.
- 432 Choi, Y., Wang, Y., Zeng, T., Cunnold, D., Yang, E. S., Martin, R., Chance, K., Thouret, V., and  
433 Edgerton, E.: Springtime transitions of NO<sub>2</sub>, CO, and O<sub>3</sub> over North America: Model evaluation  
434 and analysis, *Journal of Geophysical Research: Atmospheres*, 113, 10.1029/2007JD009632,  
435 2008b.
- 436 Choi, Y., Kim, H., Tong, D., and Lee, P.: Summertime weekly cycles of observed and modeled  
437 NO<sub>x</sub> and O<sub>3</sub> concentrations as a function of satellite-derived ozone production sensitivity and land



- 438 use types over the Continental United States, *Atmospheric Chemistry and Physics*, 12, 6291-  
439 6307, 10.5194/acp-12-6291-2012, 2012.
- 440 Crouse, D. L., Peters, P. A., Hystad, P., Brook, J. R., van Donkelaar, A., Martin, R. V.,  
441 Villeneuve, P. J., Jerrett, M., Goldberg, M. S., and Pope III, C. A.: Ambient PM<sub>2.5</sub>, O<sub>3</sub>, and NO<sub>2</sub>  
442 exposures and associations with mortality over 16 years of follow-up in the Canadian Census  
443 Health and Environment Cohort (CanCHEC), *Environmental health perspectives*, 123, 1180,  
444 10.1289/ehp.1409276, 2015.
- 445 De Gouw, J. A., Parrish, D. D., Frost, G. J., and Trainer, M.: Reduced emissions of CO<sub>2</sub>, NO<sub>x</sub>,  
446 and SO<sub>2</sub> from US power plants owing to switch from coal to natural gas with combined cycle  
447 technology, *Earth's Future*, 2, 75-82, 10.1002/2013EF000196, 2014.
- 448 Drosoglou, T., Bais, A. F., Zyrichidou, I., Kouremeti, N., Poupkou, A., Liora, N., Giannaros, C.,  
449 Koukouli, M. E., Balis, D., and Melas, D.: Comparisons of ground-based tropospheric NO<sub>2</sub>  
450 MAX-DOAS measurements to satellite observations with the aid of an air quality model over the  
451 Thessaloniki area, Greece, *Atmospheric Chemistry and Physics*, 17, 5829-5849, 10.5194/acp-17-  
452 5829-2017, 2017.
- 453 Drosoglou, T., Koukouli, M. E., Kouremeti, N., Bais, A. F., Zyrichidou, I., Balis, D., Xu, J., and  
454 Li, A.: MAX-DOAS NO<sub>2</sub> observations over Guangzhou, China; ground-based and satellite  
455 comparisons, *Atmospheric Measurement Techniques*, 11, 2239-2255, 10.5194/amt-11-2239-  
456 2018, 2018.
- 457 EPA: PROFILE OF VERSION 1 OF THE 2014 NATIONAL EMISSIONS INVENTORY, U.S.  
458 Environmental Protection Agency, 2017.
- 459 Air Pollutant Emissions Trends Data: [https://www.epa.gov/air-emissions-inventories/air-](https://www.epa.gov/air-emissions-inventories/air-pollutant-emissions-trends-data)  
460 [pollutant-emissions-trends-data](https://www.epa.gov/air-emissions-inventories/air-pollutant-emissions-trends-data), 2018.
- 461 Fisher, J. A., Jacob, D. J., Travis, K. R., Kim, P. S., Marais, E. A., Chan Miller, C., Yu, K., Zhu,  
462 L., Yantosca, R. M., and Sulprizio, M. P.: Organic nitrate chemistry and its implications for  
463 nitrogen budgets in an isoprene-and monoterpene-rich atmosphere: constraints from aircraft  
464 (SEAC<sup>4</sup>RS) and ground-based (SOAS) observations in the Southeast US, *Atmospheric chemistry*  
465 *and physics*, 16, 5969-5991, 10.5194/acp-16-5969-2016, 2016.
- 466 Greenberg, N., Carel, R. S., Derazne, E., Bibi, H., Shpriz, M., Tzur, D., and Portnov, B. A.:  
467 Different effects of long-term exposures to SO<sub>2</sub> and NO<sub>2</sub> air pollutants on asthma severity in  
468 young adults, *Journal of Toxicology and Environmental Health, Part A*, 79, 342-351,  
469 10.1080/15287394.2016.1153548, 2016.
- 470 Greenberg, N., Carel, R. S., Derazne, E., Tiktinsky, A., Tzur, D., and Portnov, B. A.: Modeling  
471 long-term effects attributed to nitrogen dioxide (NO<sub>2</sub>) and sulfur dioxide (SO<sub>2</sub>) exposure on  
472 asthma morbidity in a nationwide cohort in Israel, *Journal of Toxicology and Environmental*  
473 *Health, Part A*, 80, 326-337, 10.1080/15287394.2017.1313800, 2017.
- 474 Gu, D., Wang, Y., Smeltzer, C., and Liu, Z.: Reduction in NO<sub>x</sub> emission trends over China:  
475 Regional and seasonal variations, *Environmental science & technology*, 47, 12912-12919,  
476 10.1021/es401727e, 2013.



- 477 Gu, D., Wang, Y., Smeltzer, C., and Boersma, K. F.: Anthropogenic emissions of NO<sub>x</sub> over  
478 China: Reconciling the difference of inverse modeling results using GOME - 2 and OMI  
479 measurements, *Journal of Geophysical Research: Atmospheres*, 119, 7732-7740,  
480 10.1002/2014JD021644, 2014.
- 481 Gu, D., Wang, Y., Yin, R., Zhang, Y., and Smeltzer, C.: Inverse modelling of NO<sub>x</sub> emissions over  
482 eastern China: uncertainties due to chemical non-linearity, *Atmos. Meas. Tech.*, 9, 5193-5201,  
483 10.5194/amt-9-5193-2016, 2016.
- 484 Guenther, A. B., Jiang, X., Heald, C. L., Sakulyanontvittaya, T., Duhl, T., Emmons, L. K., and  
485 Wang, X.: The Model of Emissions of Gases and Aerosols from Nature version 2.1  
486 (MEGAN2.1): an extended and updated framework for modeling biogenic emissions,  
487 10.5194/gmd-5-1471-2012, 2012.
- 488 Hassler, B., McDonald, B. C., Frost, G. J., Borbon, A., Carslaw, D. C., Civerolo, K., Granier, C.,  
489 Monks, P. S., Monks, S., and Parrish, D. D.: Analysis of long - term observations of NO<sub>x</sub> and CO  
490 in megacities and application to constraining emissions inventories, *Geophysical Research*  
491 *Letters*, 43, 9920-9930, 10.1002/2016GL069894, 2016.
- 492 Heinrich, J., Thiering, E., Rzehak, P., Krämer, U., Hochadel, M., Rauchfuss, K. M., Gehring, U.,  
493 and Wichmann, H.-E.: Long-term exposure to NO<sub>2</sub> and PM<sub>10</sub> and all-cause and cause-specific  
494 mortality in a prospective cohort of women, *Occup Environ Med*, 70, 179-186, 10.1136/oemed-  
495 2012-100876, 2013.
- 496 Jiang, Z., McDonald, B. C., Worden, H., Worden, J. R., Miyazaki, K., Qu, Z., Henze, D. K.,  
497 Jones, D. B. A., Arellano, A. F., and Fischer, E. V.: Unexpected slowdown of US pollutant  
498 emission reduction in the past decade, *Proceedings of the National Academy of Sciences*,  
499 201801191, 10.1073/pnas.1801191115, 2018.
- 500 Kampa, M., and Castanas, E.: Human health effects of air pollution, *Environmental pollution*,  
501 151, 362-367, 10.1016/j.envpol.2007.06.012, 2008.
- 502 Kebabian, P. L., Herndon, S. C., and Freedman, A.: Detection of nitrogen dioxide by cavity  
503 attenuated phase shift spectroscopy, *Analytical chemistry*, 77, 724-728, 10.1021/ac048715y,  
504 2005.
- 505 Koo, J.-H., Wang, Y., Kurosu, T. P., Chance, K., Rozanov, A., Richter, A., Oltmans, S. J.,  
506 Thompson, A. M., Hair, J. W., and Fenn, M. A.: Characteristics of tropospheric ozone depletion  
507 events in the Arctic spring: analysis of the ARCTAS, ARCPAC, and ARCIONS measurements  
508 and satellite BrO observations, *Atmospheric Chemistry and Physics*, 12, 9909-9922, 10.5194/acp-  
509 12-9909-2012, 2012.
- 510 Krotkov, N. A., Lamsal, L. N., Celarier, E. A., Swartz, W. H., Marchenko, S. V., Bucsela, E. J.,  
511 Chan, K. L., Wenig, M., and Zara, M.: The version 3 OMI NO<sub>2</sub> standard product, *Atmospheric*  
512 *Measurement Techniques*, 10, 3133-3149, 10.5194/amt-10-3133-2017, 2017.
- 513 Lamsal, L. N., Martin, R. V., Padmanabhan, A., Van Donkelaar, A., Zhang, Q., Sioris, C. E.,  
514 Chance, K., Kurosu, T. P., and Newchurch, M. J.: Application of satellite observations for timely



- 515 updates to global anthropogenic NO<sub>x</sub> emission inventories, *Geophysical Research Letters*, 38,  
516 10.1029/2010GL046476, 2011.
- 517 Lamsal, L. N., Duncan, B. N., Yoshida, Y., Krotkov, N. A., Pickering, K. E., Streets, D. G., and  
518 Lu, Z.: US NO<sub>2</sub> trends (2005–2013): EPA Air Quality System (AQS) data versus improved  
519 observations from the Ozone Monitoring Instrument (OMI), *Atmospheric Environment*, 110,  
520 130-143, 10.1016/j.atmosenv.2015.03.055, 2015.
- 521 Laughner, J. L., Zhu, Q., and Cohen, R. C.: The Berkeley High Resolution Tropospheric NO<sub>2</sub>  
522 product, *Earth System Science Data*, 10, 2069-2095, 10.5194/essd-10-2069-2018, 2018.
- 523 Li, J., Mao, J., Fiore, A. M., Cohen, R. C., Crouse, J. D., Teng, A. P., Wennberg, P. O., Lee, B.  
524 H., Lopez-Hilfiker, F. D., and Thornton, J. A.: Decadal changes in summertime reactive oxidized  
525 nitrogen and surface ozone over the Southeast United States, *Atmospheric Chemistry and*  
526 *Physics*, 18, 2341-2361, 10.5194/acp-18-2341-2018, 2018.
- 527 Li, J., Wang, Y., and Qu, H.: Dependence of summertime surface ozone on NO<sub>x</sub> and VOC  
528 emissions over the United States: Peak time and value, *Geophysical Research Letters*, 46,  
529 10.1029/2018gl081823, 2019.
- 530 Liu, Z., Wang, Y., Vrekoussis, M., Richter, A., Wittrock, F., Burrows, J. P., Shao, M., Chang, C.  
531 C., Liu, S. C., and Wang, H.: Exploring the missing source of glyoxal (CHOCHO) over China,  
532 *Geophysical Research Letters*, 39, 10.1029/2012GL051645, 2012.
- 533 Liu, Z., Wang, Y., Costabile, F., Amoroso, A., Zhao, C., Huey, L. G., Stickel, R., Liao, J., and  
534 Zhu, T.: Evidence of aerosols as a media for rapid daytime HONO production over China,  
535 *Environmental science & technology*, 48, 14386-14391, 10.1021/es504163z, 2014.
- 536 McDonald, B., McKeen, S., Cui, Y. Y., Ahmadov, R., Kim, S.-W., Frost, G. J., Pollack, I.,  
537 Peischl, J., Ryerson, T. B., and Holloway, J.: Modeling Ozone in the Eastern US using a Fuel-  
538 Based Mobile Source Emissions Inventory, *Environmental science & technology*,  
539 10.1021/acs.est.8b00778, 2018.
- 540 Miyazaki, K., Eskes, H., Sudo, K., Boersma, K. F., Bowman, K., and Kanaya, Y.: Decadal  
541 changes in global surface NO<sub>x</sub> emissions from multi-constituent satellite data assimilation,  
542 *Atmos. Chem. Phys.*, 17, 807-837, 10.5194/acp-17-807-2017, 2017.
- 543 Myhre, G., Shindell, D., Bréon, F.-M., Collins, W., Fuglestvedt, J., Huang, J., Koch, D.,  
544 Lamarque, J.-F., Lee, D., Mendoza, B., Nakajima, T., Robock, A., Stephens, G., Takemura, T.,  
545 and Zhang, H.: Anthropogenic and natural radiative forcing, in: *Climate change 2013: The*  
546 *Physical Science Basis. Contribution of Working Group I to the Fifth Assessment Report of the*  
547 *Intergovernmental Panel on Climate Change*, Cambridge University Press, Cambridge, United  
548 Kingdom and New York, NY, USA, 659-740, 2013.
- 549 Pandey, J. S., Kumar, R., and Devotta, S.: Health risks of NO<sub>2</sub>, SPM and SO<sub>2</sub> in Delhi (India),  
550 *Atmospheric Environment*, 39, 6868-6874, 10.1016/j.atmosenv.2005.08.004, 2005.
- 551 Russell, A. R., Valin, L. C., and Cohen, R. C.: Trends in OMI NO<sub>2</sub> observations over the United  
552 States: effects of emission control technology and the economic recession, *Atmospheric*  
553 *Chemistry and Physics*, 12, 12197-12209, 10.5194/acp-12-12197-2012, 2012.



- 554 Seinfeld, J. H., and Pandis, S. N.: Atmospheric chemistry and physics: from air pollution to  
555 climate change, John Wiley & Sons, Inc, Hoboken, New Jersey, 2016.
- 556 Silvern, R. F., Jacob, D. J., Mickley, L. J., Sulprizio, M. P., Travis, K. R., Marais, E. A., Cohen,  
557 R. C., Laughner, J. L., Choi, S., Joiner, J., and Lamsal, L. N.: Using satellite observations of  
558 tropospheric NO<sub>2</sub> columns to infer long-term trends in US NO<sub>x</sub> emissions: the importance of  
559 accounting for the free tropospheric NO<sub>2</sub> background, *Atmos. Chem. Phys. Discuss.*, 2019, 1-26,  
560 10.5194/acp-2019-168, 2019.
- 561 Singh, A., and Agrawal, M.: Acid rain and its ecological consequences, *Journal of Environmental*  
562 *Biology*, 29, 15, 2007.
- 563 Tong, D., Lamsal, L., Pan, L., Ding, C., Kim, H., Lee, P., Chai, T., Pickering, K. E., and Stajner,  
564 I.: Long-term NO<sub>x</sub> trends over large cities in the United States during the great recession:  
565 Comparison of satellite retrievals, ground observations, and emission inventories, *Atmospheric*  
566 *Environment*, 107, 70-84, 10.1016/j.atmosenv.2015.01.035, 2015.
- 567 Valin, L. C., Russell, A. R., Hudman, R. C., and Cohen, R. C.: Effects of model resolution on the  
568 interpretation of satellite NO<sub>2</sub> observations, *Atmospheric Chemistry and Physics*, 11, 11647-  
569 11655, 10.5194/acp-11-11647-2011, 2011.
- 570 Wang, Y., Choi, Y., Zeng, T., Davis, D., Buhr, M., Huey, L. G., and Neff, W.: Assessing the  
571 photochemical impact of snow NO<sub>x</sub> emissions over Antarctica during ANTCI 2003, *Atmospheric*  
572 *Environment*, 41, 3944-3958, 10.1016/j.atmosenv.2007.01.056, 2007.
- 573 Wang, Y., Beirle, S., Lampel, J., Koukouli, M., De Smedt, I., Theys, N., Ang, L., Wu, D., Xie, P.,  
574 and Liu, C.: Validation of OMI, GOME-2A and GOME-2B tropospheric NO<sub>2</sub>, SO<sub>2</sub> and HCHO  
575 products using MAX-DOAS observations from 2011 to 2014 in Wuxi, China: investigation of the  
576 effects of priori profiles and aerosols on the satellite products, *Atmospheric Chemistry and*  
577 *Physics*, 17, 5007, 10.5194/acp-17-5007-2017, 2017.
- 578 Weinmayr, G., Romeo, E., De Sario, M., Weiland, S. K., and Forastiere, F.: Short-term effects of  
579 PM<sub>10</sub> and NO<sub>2</sub> on respiratory health among children with asthma or asthma-like symptoms: a  
580 systematic review and meta-analysis, *Environmental health perspectives*, 118, 449-457,  
581 10.1289/ehp.0900844, 2009.
- 582 Xing, J., Pleim, J., Mathur, R., Pouliot, G., Hogrefe, C., Gan, C. M., and Wei, C.: Historical  
583 gaseous and primary aerosol emissions in the United States from 1990 to 2010, *Atmos. Chem.*  
584 *Phys.*, 13, 7531-7549, 10.5194/acp-13-7531-2013, 2013.
- 585 Yang, Q., Wang, Y., Zhao, C., Liu, Z., Gustafson Jr, W. I., and Shao, M.: NO<sub>x</sub> emission reduction  
586 and its effects on ozone during the 2008 Olympic Games, *Environmental science & technology*,  
587 45, 6404-6410, 10.1021/es200675v, 2011.
- 588 Yienger, J. J., and Levy, H.: Empirical model of global soil - biogenic NO<sub>x</sub> emissions, *Journal of*  
589 *Geophysical Research: Atmospheres*, 100, 11447-11464, 10.1029/95JD00370, 1995.
- 590 Yu, K., Jacob, D. J., Fisher, J. A., Kim, P. S., Marais, E. A., Miller, C. C., Travis, K. R., Zhu, L.,  
591 Yantosca, R. M., and Sulprizio, M. P.: Sensitivity to grid resolution in the ability of a chemical



- 592 transport model to simulate observed oxidant chemistry under high-isoprene conditions,  
593 Atmospheric Chemistry and Physics, 16, 4369-4378, 10.5194/acp-16-4369-2016, 2016.
- 594 Zara, M., Boersma, K. F., De Smedt, I., Richter, A., Peters, E., Van Geffen, J. H. G. M., Beirle,  
595 S., Wagner, T., Van Roozendaal, M., and Marchenko, S.: Improved slant column density retrieval  
596 of nitrogen dioxide and formaldehyde for OMI and GOME-2A from QA4ECV: intercomparison,  
597 uncertainty characterization, and trends, Meas. Tech. Discuss, 1-47, 10.5194/amt-11-4033-2018,  
598 2018.
- 599 Zhang, R., Wang, Y., He, Q., Chen, L., Zhang, Y., Qu, H., Smeltzer, C., Li, J., Alvarado, L., and  
600 Vrekoussis, M.: Enhanced trans-Himalaya pollution transport to the Tibetan Plateau by cut-off  
601 low systems, Atmospheric Chemistry and Physics, 17, 3083-3095, 10.5194/acp-17-3083-2017,  
602 2017.
- 603 Zhang, R., Wang, Y., Smeltzer, C., Qu, H., Koshak, W., and Boersma, K. F.: Comparing OMI-  
604 based and EPA AQS in situ NO<sub>2</sub> trends: towards understanding surface NO<sub>x</sub> emission changes,  
605 Atmospheric Measurement Techniques, 11, 3955-3967, 10.5194/amt-11-3955-2018, 2018.
- 606 Zhang, Y., and Wang, Y.: Climate-driven ground-level ozone extreme in the fall over the  
607 Southeast United States, Proceedings of the National Academy of Sciences, 113, 10025-10030,  
608 10.1073/pnas.1602563113, 2016.
- 609 Zhao, C., and Wang, Y.: Assimilated inversion of NO<sub>x</sub> emissions over east Asia using OMI NO<sub>2</sub>  
610 column measurements, Geophysical Research Letters, 36, 10.1029/2008GL037123, 2009.
- 611 Zhao, C., Wang, Y., Choi, Y., and Zeng, T.: Summertime impact of convective transport and  
612 lightning NO<sub>x</sub> production over North America: modeling dependence on meteorological  
613 simulations, Atmospheric Chemistry and Physics, 9, 4315-4327, 10.5194/acp-9-4315-2009,  
614 2009a.
- 615 Zhao, C., Wang, Y., and Zeng, T.: East China plains: A “basin” of ozone pollution,  
616 Environmental science & technology, 43, 1911-1915, 10.1021/es8027764, 2009b.
- 617 Zhao, C., Wang, Y., Yang, Q., Fu, R., Cunnold, D., and Choi, Y.: Impact of East Asian summer  
618 monsoon on the air quality over China: View from space, Journal of Geophysical Research:  
619 Atmospheres, 115, 10.1029/2009JD012745, 2010.
- 620



**Table 1.** Summary of trends of satellite NO<sub>2</sub> TVCD products, NO<sub>2</sub> surface measurements, and EPA anthropogenic NO<sub>x</sub> emissions during from different studies

Studies	Datasets	Period 1 <sup>1</sup>		Period 2		Period 3		Slowdown ratio <sup>3</sup>
		Time	Trend (yr <sup>-1</sup> ) <sup>2</sup>	Time	Trend (yr <sup>-1</sup> )	Time	Trend (yr <sup>-1</sup> )	
This study for CONUS "urban" sites <sup>4</sup>	GOME-2B <sup>5</sup> (36 × 36 km <sup>2</sup> )	2003 – 2011	-6.3 ± 1.1%	2013 – 2017	-8.2 ± 3.0%	2013 – 2017	-8.2 ± 3.0%	-29%
	SCIAMACHY (36 × 36 km <sup>2</sup> )	2005 – 2011	-8.6 ± 1.2%	2011 – 2016	-6.1 ± 3.6%	2011 – 2016	-6.1 ± 3.6%	-46%
	OMI-NASA (36 × 36 km <sup>2</sup> )	2005 – 2011	-8.2 ± 1.3%	2011 – 2016	-4.4 ± 1.6%	2011 – 2016	-4.4 ± 1.6%	-46%
	OMI-BEHR (36 × 36 km <sup>2</sup> )	2005 – 2011	-7.7 ± 1.4%	2011 – 2017	-5.1 ± 0.3%	2011 – 2017	-5.1 ± 0.3%	-22%
	OMI-QA4ECV (36 × 36 km <sup>2</sup> )	2003 – 2011	-6.5 ± 0.8%	2013 – 2017	-10.2 ± 2.9%	2013 – 2017	-10.2 ± 2.9%	
This study for AQS "urban" sites	GOME-2B (36 × 36 km <sup>2</sup> )	2003 – 2011	-7.6 ± 1.1%	2011 – 2016	-7.2 ± 3.8%	2011 – 2016	-7.2 ± 3.8%	-20%
	SCIAMACHY (36 × 36 km <sup>2</sup> )	2005 – 2011	-9.0 ± 0.8%	2011 – 2016	-6.2 ± 2.6%	2011 – 2016	-6.2 ± 2.6%	-30%
	OMI-NASA (36 × 36 km <sup>2</sup> )	2005 – 2011	-8.9 ± 0.3%	2011 – 2017	-5.4 ± 0.9%	2011 – 2017	-5.4 ± 0.9%	-40%
	OMI-BEHR (36 × 36 km <sup>2</sup> )	2005 – 2011	-9.0 ± 0.8%	2011 – 2017	-5.9 ± 0.8%	2011 – 2017	-5.9 ± 0.8%	-9%
	OMI-QA4ECV (36 × 36 km <sup>2</sup> )	2003 – 2011	-6.5 ± 1.2%	2011 – 2017	-3 ± 4% (-3.0%)	2011 – 2017	-3 ± 4% (-3.0%)	-52%
(Russell et al., 2012) <sup>8</sup>	BEHR v2.1 NO <sub>2</sub> TVCD (0.05°×0.05°)	2005 – 2007	-6 ± 5% (-6.2%) <sup>y</sup>	2007 – 2009	-8 ± 5% (-8.4%)	2009 – 2011	-3 ± 4% (-3.0%)	-60%
(Tong et al., 2015) <sup>10</sup>	Updated EPA NO <sub>x</sub> emissions	2005 – 2007	-6.0%	2007 – 2009	-10.0%	2009 – 2011	-2.4%	
	NASA v2.1 NO <sub>2</sub> TVCD (pixels < 50 × 24 km <sup>2</sup> )	2005 – 2007	-7.3% (-7.6%)	2008 – 2009	-9.2% (-11.4%)	2010 – 2012	-2.8% (-4.4%)	-42%
	BEHR v2.1 NO <sub>2</sub> TVCD (pixels < 50 × 24 km <sup>2</sup> )	2005 – 2007	-8.9% (-9.3%)	2008 – 2009	-9.1% (-11.8%)	2010 – 2012	-3.6% (-6.0%)	-35%
	NO <sub>2</sub> surface VMR	2005 – 2007	-6.0% (-6.2%)	2008 – 2009	-10.8% (-13.2%)	2010 – 2012	-3.4% (-5.4%)	-13%
	Updated EPA NO <sub>x</sub> emissions	2005 – 2007	-6.0%	2008 – 2009	-10.0%	2010 – 2012	-3.4%	-43%
(Lamsal et al., 2015) <sup>11</sup>	NASA v2.1 NO <sub>2</sub> TVCD (0.1°×0.1°)	2005 – 2008	-4.8 ± 1.9% (-5.1%)	2010 – 2013	-1.2 ± 1.2% (-1.2%)	2010 – 2013	-2.1 ± 1.4% (-2.1%)	-76%
	NO <sub>2</sub> surface VMR	2005 – 2008	-3.7 ± 1.5% (-3.8%)	2010 – 2013	-2.1 ± 1.4% (-2.1%)	2010 – 2013	-2.1 ± 1.4% (-2.1%)	-45%
	Updated EPA NO <sub>x</sub> emissions	2005 – 2008	-6.4%	2010 – 2013	-4.0%	2010 – 2013	-4.0%	-38%
	NASA v3 NO <sub>2</sub> TVCD (0.5°×0.667°)	2005 – 2009	-10.2 ± 1.8% (-9.8%)	2011 – 2015	-3.2 ± 1.6% (-3.2%)	2011 – 2015	-3.2 ± 1.6% (-3.2%)	-67%
	QA4ECV v2 NO <sub>2</sub> TVCD (0.5°×0.667°)	2005 – 2009	-9.6 ± 1.7% (-9.3%)	2011 – 2015	-2.6 ± 1.8% (-2.6%)	2011 – 2015	-2.6 ± 1.8% (-2.6%)	-72%
(Jiang et al., 2018) <sup>11</sup>	BEHR v2.1 NO <sub>2</sub> TVCD (0.5°×0.667°)	2005 – 2009	-8.5 ± 1.8% (-8.2%)	2011 – 2015	-2.1 ± 1.6% (-2.1%)	2011 – 2015	-2.1 ± 1.6% (-2.1%)	-74%
	NO <sub>2</sub> surface VMR	2005 – 2009	-6.6 ± 1.4% (-6.4%)	2011 – 2015	-2.6 ± 1.5% (-2.6%)	2011 – 2015	-2.6 ± 1.5% (-2.6%)	-59%
	Updated EPA NO <sub>x</sub> emissions	2005 – 2009	-7.8%	2011 – 2015	-5.0%	2011 – 2015	-5.0%	-36%

<sup>1</sup> Since different studies used different time division methods, we list the period of each study in the table.

<sup>2</sup> Trends are based on an exponential model  $E(y) = E_0 \times r^{y-y_0}$ ; "y" denotes year and "y<sub>0</sub>" denotes the initial year; "E(y)" denotes the value at the initial year; "r-1" is the relative trend).

<sup>3</sup> Slowdown ratios = Trend in "period 3" / Trend in "period 1" - 1.

<sup>4</sup> Trends in our study are calculated based on the national seasonal trends shown in Table 3.

<sup>5</sup> The information on satellite products used in this study is summarized in Table S2.

<sup>6</sup> We updated EPA anthropogenic NO<sub>x</sub> emissions with the newest Continuous Emission Monitoring Systems (CEMS) datasets. Figure S1 shows the comparison between our updated and original EPA anthropogenic NO<sub>x</sub> emissions (EPA, 2018).

<sup>7</sup> Denote the averaged trends of 13:00 and 10:00 LT based on the values in Table 3.



629 <sup>8</sup> The study used NO<sub>2</sub> TVCD from urban and power plant grid cells across the U.S.  
630 <sup>9</sup> Since previous studies used linear models to calculate trends and the results are sensitive to their calculation methods and the selection of initial years, we recalculate the trends based on the above exponential model, which makes all the results  
631 consistent. Our results are those bold numbers inside the parentheses, while the numbers in normal fonts are from the original publications.  
632 <sup>10</sup> The study uses NO<sub>2</sub> TVCD and surface concentrations from Los Angeles, Dallas, Houston, Atlanta, Philadelphia, Washington, D.C., New York, and Boston.  
633 <sup>11</sup> The two studies used the EPA Air Quality System (AQS) NO<sub>2</sub> surface measurements and coincident satellite NO<sub>2</sub> TVCD data over the U.S.



634 **Table 2.** Properties of urban and rural regions in July 2011

type	Surface area fraction <sup>1</sup>	Anthropogenic NO <sub>x</sub> emissions ( $\times 10^{10}$ molecules cm <sup>-2</sup> s <sup>-1</sup> )	$\beta$ at 13:00 – 14:00 LT	$\gamma$ at 13:00 – 14:00 LT	$\beta$ at 10:00 – 11:00 LT	$\gamma$ at 10:00 – 11:00 LT
Urban/CONUS <sup>2</sup>	17.3%	29.9	2.3 ± 0.9	1.4 ± 0.3	2.4 ± 1.8	1.5 ± 1.0
Rural/CONUS	82.7%	2.7	8.1 ± 8.7	3.1 ± 3.9	5.9 ± 8.0	2.8 ± 5.8
Urban/AQS	87.7%	71.0	1.5 ± 0.7	1.2 ± 0.4	1.7 ± 1.0	1.3 ± 0.5
Rural/AQS	12.3%	5.7	5.0 ± 2.0	2.5 ± 1.3	4.3 ± 3.2	2.7 ± 2.6

635 <sup>1</sup>“Fraction” denotes the percentages of “urban” or “rural” data points for the whole CONUS or all AQS sites.

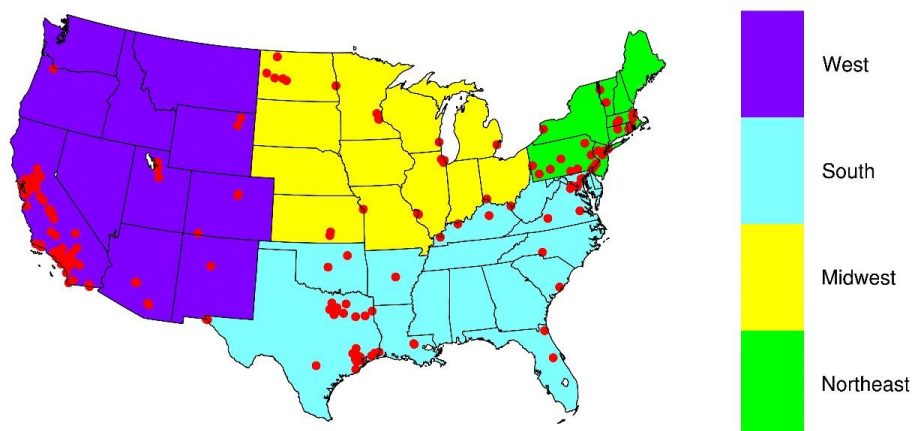
636 <sup>2</sup>“Urban-CONUS” denote CONUS “urban” grid cells; “Urban-AQS” denote AQS “urban” site grid cells.



**Table 3.** Summary of national trends of updated EPA anthropogenic NO<sub>x</sub> emissions, AQS NO<sub>2</sub> surface concentrations at 13:00 – 14:00 and 10:00 – 11:00 LT, and satellite NO<sub>2</sub> TVCD products for 4 seasons during different periods<sup>1</sup>

		Spring			Summer			Autumn			Winter		
		AQS site	CONUS	AQS site	CONUS	AQS site	CONUS	AQS site	CONUS	AQS site	CONUS	AQS site	CONUS
AQS NO <sub>2</sub> VMR at 13:00–14:00	2003–2011	-7.3 ± 1.4%		-7.4 ± 0.9%		-6.7 ± 1.8%		-5.2 ± 0.8%		-6.0 ± 2.8%		-5.2 ± 0.8%	
	2011–2017	-5.3 ± 1.6%		-6.4 ± 1.2%		-7.3 ± 2.5%		-6.0 ± 2.8%		-7.3 ± 2.5%		-6.0 ± 2.8%	
AQS NO <sub>2</sub> VMR at 10:00–11:00	2003–2011	-7.1 ± 1.6%		-7.6 ± 1.5%		-6.2 ± 2.2%		-4.4 ± 1.6%		-6.3 ± 2.5%		-5.2 ± 2.4%	
	2011–2017	-4.4 ± 1.4%		-6.1 ± 1.8%		-6.3 ± 2.5%		-5.2 ± 2.4%		-6.3 ± 2.5%		-5.2 ± 2.4%	
SCIAMACHY	2003–2011	-8.8 ± 3.4%	-6.9 ± 1.1%	-8.2 ± 1.6%	-5.2 ± 1.2%	-6.8 ± 2.4%	-5.6 ± 2.1%	-6.4 ± 7.4%	-7.5 ± 5.5%				
	2011–2017												
GOME2B	2003–2011												
	2013–2017	-10.2 ± 7.8%	-8.3 ± 16.9%	-6.4 ± 14.0%	-5.3 ± 4.0%	-10.5 ± 41.6%	-6.9 ± 13.2%	-13.6 ± 15.1%	-12.3 ± 78.9%				
OMI-QA4ECV	2005–2011	-9.3 ± 5.6%	-8.3 ± 4.6%	-8.3 ± 2.4%	-5.9 ± 5.2%	-10.0 ± 4.2%	-7.4 ± 2.4%	-8.3 ± 2.1%	-9.3 ± 5.2%				
	2011–2017	-5.3 ± 6.0%	-4.3 ± 6.5%	-4.2 ± 3.0%	-4.9 ± 9.2%	-6.0 ± 1.8%	-3.8 ± 1.8%	-6.1 ± 25.6%	-3.8 ± 3.5%				
OMI-NASA	2005–2011	-9.4 ± 5.0%	-9.6 ± 5.3%	-9.4 ± 2.8%	-7.1 ± 2.9%	-9.4 ± 3.2%	-8.1 ± 2.8%	-7.8 ± 3.6%	-9.5 ± 16.6%				
	2011–2016	-4.4 ± 18.9%	-3.8 ± 7.5%	-5.7 ± 6.7%	-4.5 ± 5.3%	-6.0 ± 3.1%	-4.6 ± 3.9%	-12.8 ± 7.8%	-11.4 ± 6.6%				
OMI-BEHR	2005–2011	-9.1 ± 5.3%	-8.9 ± 5.8%	-8.7 ± 2.4%	-6.4 ± 3.2%	-9.2 ± 3.2%	-8.0 ± 3.1%	-8.5 ± 10.6%	-9.4 ± 23.0%				
	2011–2016	-3.8 ± 4.4%	-3.0 ± 4.0%	-5.4 ± 7.0%	-3.9 ± 6.6%	-5.6 ± 13.2%	-4.1 ± 14.0%	-9.9 ± 5.2%	-6.7 ± 5.9%				
EPA	2003–2011												
	2011–2017												

<sup>1</sup> We calculate trends by using the exponential model described in Table 1.

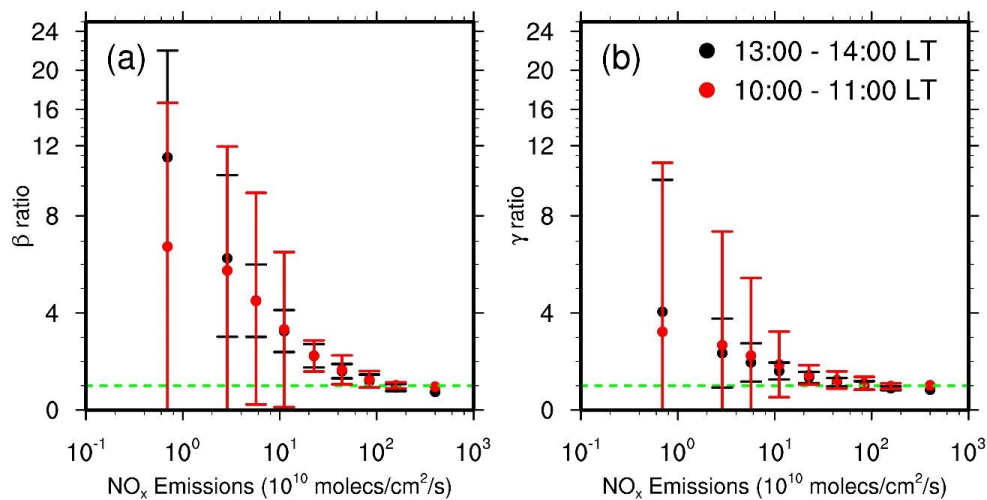


642  
643 Figure 1. Region definitions and locations of NO<sub>2</sub> surface observation sites used in this study.

644



645



646

647

648

649

650

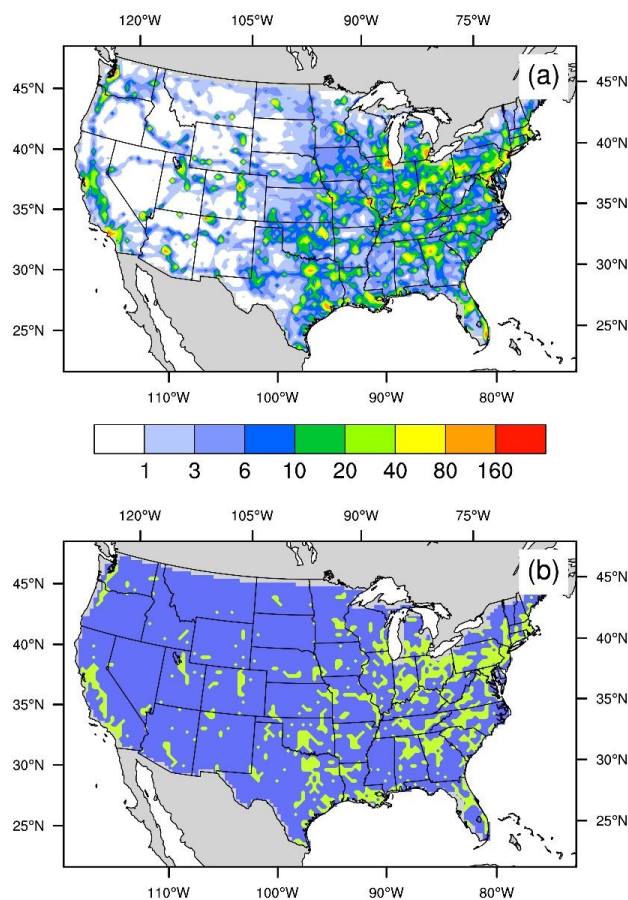
651

652

653

Figure 2. Distributions of  $\beta$  (panel a) and  $\gamma$  (panel b) ratios as a function of anthropogenic  $\text{NO}_x$  emissions on weekdays for July 2011 over the CONUS. “13:00 – 14:00 LT” is for OMI, and “10:00 – 11:00” LT is for SCIAMACHY and GOME-2A/2B. The data are binned into nine groups based on anthropogenic  $\text{NO}_x$  emissions:  $E \in (0, 2^1), [2^1, 2^2), [2^2, 2^3), [2^3, 2^4), [2^4, 2^5), [2^5, 2^6), [2^6, 2^7), [2^7, 2^8), [2^8, 2^9) \times 10^{10}$  molecules  $\text{cm}^{-2} \text{s}^{-1}$ . Here,  $(0, 2^1)$  denotes  $0 < \text{emissions} < 2^1$ , and  $[2^1, 2^2)$  denotes  $2^1 \leq \text{emissions} < 2^2$ , similar to other intervals. The green dashed line denotes a value of 1. Error bars denote standard deviations.

654

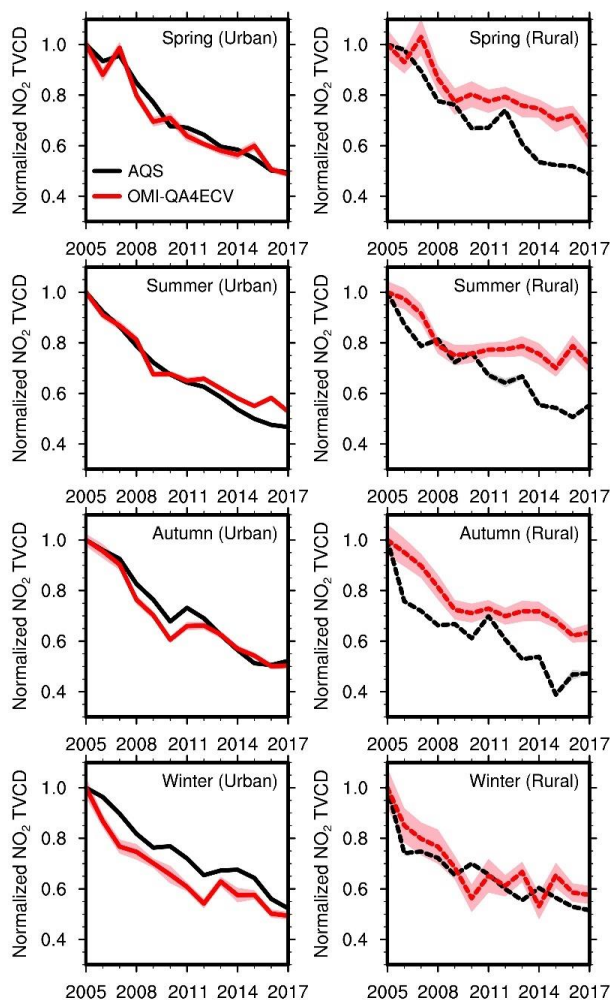


655  
656 Figure 3. Spatial distributions of (a) anthropogenic NO<sub>x</sub> emissions (unit: 10<sup>10</sup> molecules cm<sup>-2</sup> s<sup>-1</sup>)  
657 and (b) “urban” regions satisfying our selection criteria. In (b), light green and blue denote the  
658 resulting urban and rural regions, respectively.

659

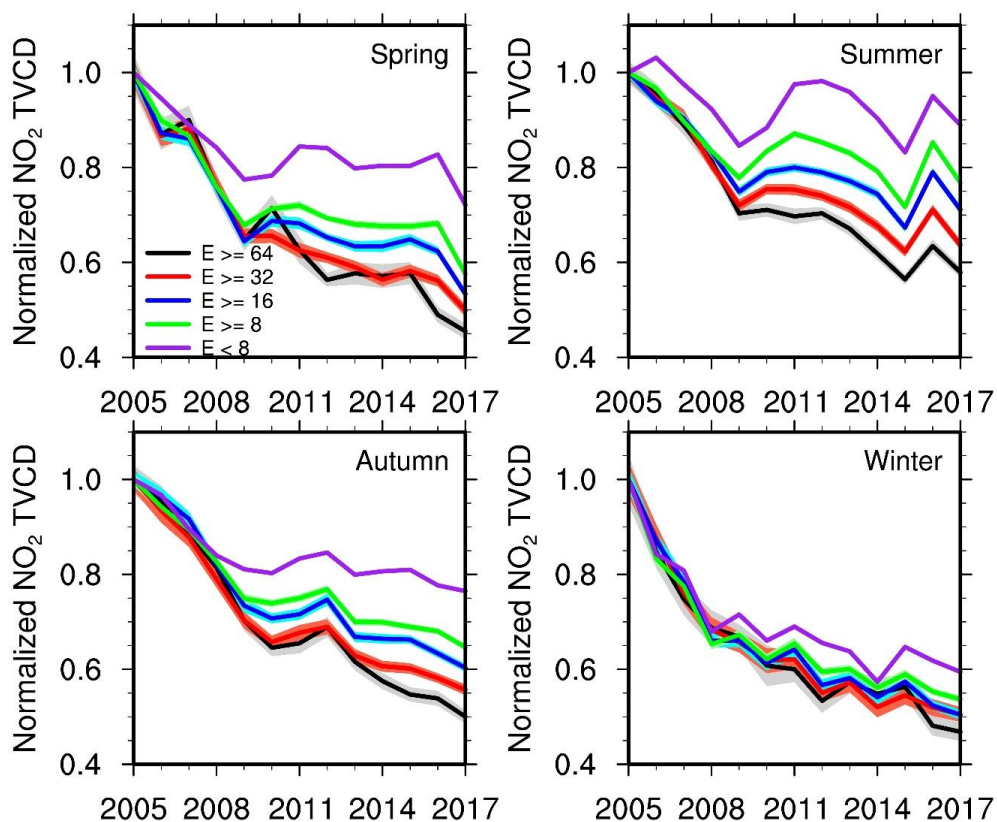


660



661  
662 Figure 4. Relative annual variations of AQS NO<sub>2</sub> surface concentrations and coincident OMI-  
663 QA4ECV NO<sub>2</sub> TVCD in each season from 2005 – 2017 for urban (left panel) and rural (right  
664 panel) regions. The observation data are scaled by the corresponding 2005 values. Black and red  
665 lines denote AQS surface observations and OMI-QA4ECV NO<sub>2</sub> TVCDs, respectively. Shading in  
666 a lighter color is added to show the standard deviation of the results; when uncertainty is small  
667 due in part to a large number of data points, shading area may not show up.

668



669

670

671 Figure 5. Relative annual variations of OMI-QA4ECV NO<sub>2</sub> TVCD for different anthropogenic

672 NO<sub>x</sub>-emission groups in each season from 2005 – 2017. “E ≥ 64” denotes grid cells with

673 anthropogenic NO<sub>x</sub> emissions equal to or larger than 64 × 10<sup>10</sup> molecules cm<sup>-2</sup> s<sup>-1</sup>. “E ≥ 32” denotes grid cells

674 with anthropogenic NO<sub>x</sub> emissions equal to or larger than 32 × 10<sup>10</sup> molecules cm<sup>-2</sup> s<sup>-1</sup> but less

675 than 64 × 10<sup>10</sup> molecules cm<sup>-2</sup> s<sup>-1</sup>. “E ≥ 16” and “E ≥ 8” have similar meanings as “E ≥ 32”.

676 “E < 8” denotes grid cells with anthropogenic NO<sub>x</sub> emissions less than 8 × 10<sup>10</sup> molecules cm<sup>-2</sup> s<sup>-1</sup>.

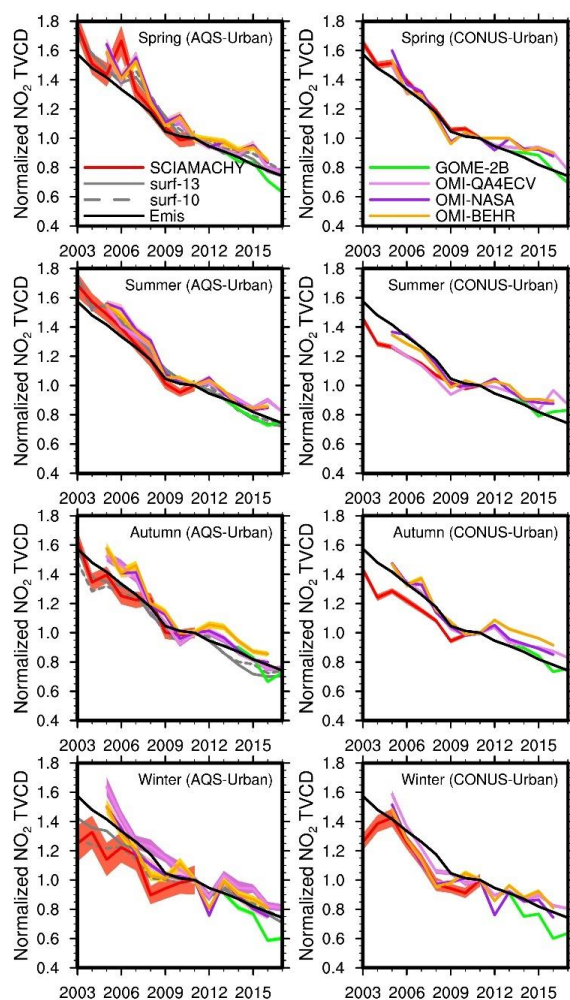
677 Shading in a lighter color is added to show the standard deviation of the results; when

678 uncertainty is small due in part to a large number of data points, shading area may not show up.

678



679

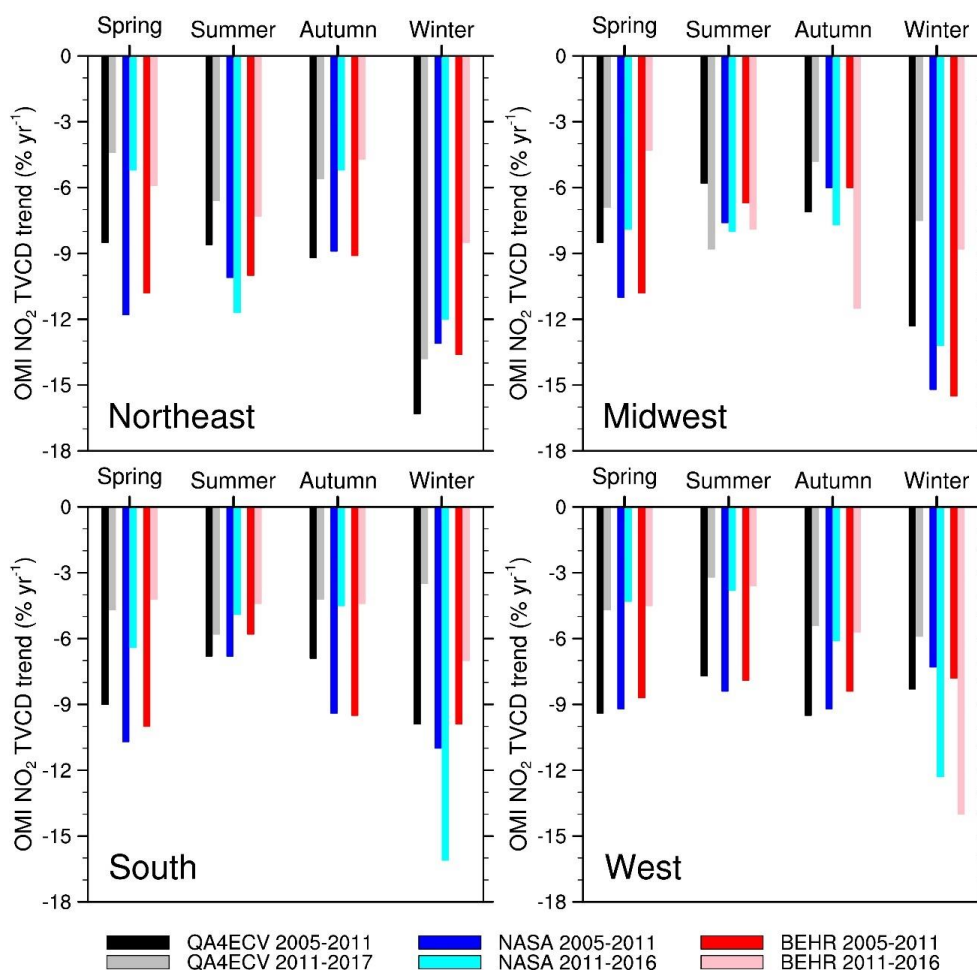


680  
681 Figure 6. Relative variations of AQS NO<sub>2</sub> surface measurements at 13:00-14:00 and 10:00-11:00  
682 LT, updated EPA anthropogenic NO<sub>x</sub> emissions, and satellite NO<sub>2</sub> TVCD data over the AQS  
683 urban sites (left column) and the CONUS urban regions (right column) for 4 seasons. AQS NO<sub>2</sub>  
684 surface measurements are not included in the right column. All datasets are scaled by their  
685 corresponding values in 2011 except for GOME-2B. For GOME-2B, we firstly normalized the  
686 values in each season to the corresponding 2013 values and plotted the relative changes from the  
687 2013 EPA point of each season to make the GOME-2B relative variations comparable to the  
688 other datasets. Shading in a lighter color is added to show the standard deviation of the results;  
689 when uncertainty is small due in part to a large number of data points, shading area may not show  
690 up.

691



692



693

694

695

696

697

698

699

Figure 7. Pre- and post-2011 OMI NO<sub>2</sub> TVCD trends for 4 seasons in the urban regions of Northeast, Midwest, South, and West. Black bars denote OMI-QA4ECV NO<sub>2</sub> TVCD trends from 2005 – 2011; gray bars denote the corresponding trends during 2011 – 2017. Blue bars denote OMI-NASA trends from 2005 – 2011; cyan bars denote NASA-OMI trends from 2011 – 2016. Red bars denote BEHR-OMI trends from 2005 – 2011; pink bars denote OMI-BEHR trends from 2011 – 2016.

700